Internal wave–turbulence pressure above sloping sea bottoms

Hans van Haren[1]

Received 1 March 2011; revised 12 September 2011; accepted 22 September 2011; published 6 December 2011.

[1] An accurate bottom pressure sensor has been moored at different sites varying from a shallow sea strait via open ocean guyots to a 1900 m deep Gulf of Mexico. All sites show more or less sloping bottom topography. Focusing on frequencies (σ) higher than tidal, the pressure records are remarkably similar, to within the 95% statistical significance bounds, in the internal gravity wave continuum (IWC) band up to buoyancy frequency N. The IWC has a relatively uniform spectral slope: $\log(P(\sigma)) = -\alpha\log(\sigma)$, $\alpha = 2 \pm 1/3$. The spectral collapse is confirmed from independent internal hydrostatic pressure estimate, which suggests a saturated IWC. For $\sigma > N$, all pressure-spectra transit to a bulge that differs in magnitude. This bulge is commonly attributed to long surface waves. For the present data it is suggested to be due to stratified turbulence–internal wave coupling, which is typically large over sloping topography. The bulge drops off at a more or less common frequency of 2–3 $\times$ 10^{-2} Hz, which is probably related with typical turbulent overturning scales.

Citation: van Haren, H. (2011), Internal wave–turbulence pressure above sloping sea bottoms, *J. Geophys. Res.*, *116*, C12004, doi:10.1029/2011JC007085.

1. Introduction

[2] It seems academic to investigate pressure variations equivalent to millimeter-centimeter water level variations, or 10–100 N m^{-2}, in 10–1000 m deep waters where hydrostatic pressures amount 10^5–10^7 N m^{-2}. Yet, as will be investigated here, they may prove useful to understand an aspect of potentially important deep ocean mixing processes of internal waves (breaking).

[3] The majority of publications on bottom pressure observations have a geological, seismic origin. Such sensors have been installed in the deep ocean to compliment land-based sensors, for example to fill gaps in tsunami warning systems. Bottom pressure usually complements the seismic more important 3 axes motion sensors, to correct for "noise." From a seismic viewpoint ocean bottom sensors are generally less accurate than land-based sensors [*Webb*, 1998]. Part of unwanted noise signal is attributable to less accurate positioning of the instrumentation at the seafloor, part is due to typical ocean motions. So far, corrections for such unwanted motions have focused on hydrostatic, generally linear wave motions. These are termed "noise," although the apparent noise has a much broader spectral appearance than spiky deterministic harmonic wave motions.

[4] A typical (deep) ocean bottom pressure spectrum (Figure 1) [e.g., *Filloux*, 1980; *Webb*, 1998] has a peak around frequency $\sigma \sim 0.1$ Hz, because of wind-driven surface waves (SW). The SW are heavily exponentially attenuated with depth and usually not observed at the bottom, except in O(100 m) shallow water (compare Table 1). This attenuation with depth is progressively less for longer, e.g., tsunami, waves, which are in the range $0.002 < \sigma < 0.03$ Hz. This "infragravity wave" (IGW) band also contains energy because of nonlinear processes from wind waves and swell [e.g., *Webb*, 1998; *Uchiyama and McWilliams*, 2008]. As waves are highly nonlinear just prior to breaking, IGW generation occurs in the nearshore surf zone, where it is strongly correlated with swell [*Herbers et al.*, 1995]. Radiation stress in a group of waves leads to the relatively low frequency modulus residual [*Longuet-Higgins and Stewart*, 1964]. The resulting long, thus weakly attenuated, waves can only propagate into the open sea and ocean. Far from coasts, IGW may also be generated locally via nonlinear interaction between swell and mesoscale motions [*Uchiyama and McWilliams*, 2008]. Debate is ongoing which is more dominant in the open ocean: local IGW generation or IGW propagation away from coasts [*Bromirski and Gerstoft*, 2009]. In all cases, a spectral gap is found between IGW and SW.

[5] At frequencies below IGW, the bottom pressure spectrum adopts a σ^{-2} dropoff rate between tides ($\sigma = 2 \times 10^{-5}$ Hz), plus their higher harmonics, and 0.002 Hz at more or less fixed power per frequency irrespective of sources and with no apparent seasonal cycle [*Filloux*, 1980]. *Webb* [1998] suggests that pressure in this band is driven directly by atmospheric fluctuations, whereas *Okihiro and Guza* [1995] suggest a modulation by tides. On the other hand, the above band is typically the inertio gravity ("internal") wave band, which is generally defined between inertial frequency f and buoyancy frequency N, for $N \gg f$. This band may transfer energy to turbulence across its natural cutoff at N, as suggested by *Filloux* [1980]. Here, we will postulate it as the "internal gravity wave continuum" (IWC) and note

[1]Physical Oceanography, Royal Netherlands Institute for Sea Research, Den Burg, Netherlands.

0148-0227/11/2011JC007085

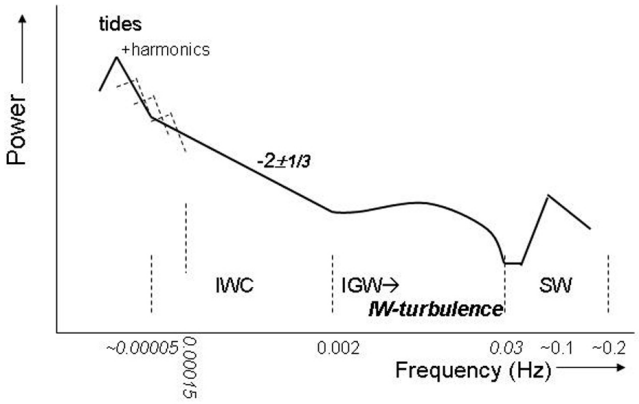

Figure 1. Sketch of bottom pressure data compiled from historic data and using common naming. IWC, internal wave continuum band; IGW, infragravity wave band; SW, surface wave band. Italicized is a new name for sloping bottom observations (IWT).

that a sharp kink in slope or a small gap rather than a clear gap is observed between IWC and IGW, in comparison with the gap between IGW and SW.

[6] The internal wave-turbulence transition has been modeled following Lagrangean (drifter) vertical velocity observations from both shallow (throughflow-sill) waters and open ocean [*D'Asaro and Lien*, 2000a, 2000b]. Their frequency spectra collapse to one with predominantly internal wave contributions and σ^0 falloff rate for $\sigma < N$ (where σ^{-2} is found for horizontal motions), and predominantly turbulence and σ^{-2} for $\sigma > N$ in highly energetic areas over topography. They also modeled shear, and its vertical wave number (m) spectrum falls off like m^{-1} in the (saturated) IWC and shows a sharp transition to a turbulence (not IGW) bulge, quite like the one in the bottom pressure frequency range in Figure 1.

[7] So far few attempts have been made to resolve physical oceanographic important dynamic parameters like nonhydrostatic pressure (due to vertical velocity accelerations; p_{nh}) and internal hydrostatic (baroclinic; p_{ih}) pressure from the internal wave band, let alone the turbulence band. Following *Moum and Smyth* [2006] (non) linear internal wave pressure variations observed at level z just above the bottom read,

$$p'(z,t) = p_{nh} + p_{ih} + p_{eh},$$
$$p_{nh} = \int_z^{\langle H \rangle} \langle \rho \rangle \frac{Dw}{Dt} d\tilde{z}; \quad p_{ih} = \int_z^{\langle H \rangle} \rho' g d\tilde{z}; \quad p_{eh} = \langle \rho \rangle g \eta, \tag{1}$$

in which p_{eh} denotes the wave's external hydrostatic pressure, ρ density, H water depth, g acceleration of gravity, w the vertical velocity, η wave-induced sea level variations

Table 1. Mooring Details[a]

	Marsdiep	Baltic Sea	Great Meteor Seamount	Equator Seamount	Gulf of Mexico
Latitude	52°59.025′N	1: 55°14.961′N; 2: 54°56.730′N; 3: 54°57.798′N	30°00.052′N	00°44.154′N	28°48′N
Longitude	04°46.876′E	1: 15°59.274′E; 2: 16°05.814′E; 3: 16°02.934′E	28°18.802′W	39°51.178′W	88°00′W
Water depth (m)	23	1: 90; 2: 67; 3: 72	549	1172	1932
Bottom slope	4.7° (sand wave)	1: 3.0° (basin); 2: 1.0° (slope); 3: 1.3° (slope)	3.9°	21°	1.5° (2′grid)
Moored period	28–31 May 2001	1: 28 Feb–4 Mar 2010; 2: 4–7 Mar 2010; 3: 7–8 Mar 2010	21 May–8 Jun 2006	5–13 Dec 2007	22 Apr–28 Jul 2005
Pressure sensor	SBE 26plus	SBE 53	SBE 53	SBE 53	SBE 53
Sampling	4 Hz: 500 s burst in 600 s sampling period	0.33 Hz continuously	0.33 Hz continuously	0.33 Hz continuously	0.067 Hz continuously
σ_{max} (Hz)	0.3	0.15	0.05	0.04	0.02
Mounting (height above bottom)	0.08 m frame	0.62 m lander	1.70 m lander	1.70 m lander	100 m from wellhead below DPS-rig
Additional instruments	ADCP, CTD	ADCP, CTD, NIOZ-T	ADCP, CM, CTD, NIOZ-T	CM, CTD, NIOZ-T	–
Current speed (m s^{-1})	0–1.4	1: 0–0.4; 2: 0–0.15; 3: 0–0.25	0–0.4	0–0.35	?
N,N_1 (Hz)	0.048, 0.016	1–3: 0.0072, 0.016	0.00057, 0.0022	0.0004, 0.0016	?
Remarks	Strong semidiurnal tidal currents; resuspension; estuarine flow/stratification	General: weak tides, inertial motions dominate; 1: storm mode 1 high-frequency internal waves 2, 3: above slope; mode 2 HF internal waves	Semidiurnal tidal thermal fronts	Semidiurnal tidal fronts/turbulence	One tropical storm and three hurricanes passed, with Cindy and Dennis directly over site; diurnal tide/inertial motions

[a]SBE = Sea-Bird Electronics; ADCP = 300 kHz RDI acoustic Doppler current profiler; CTD = conductivity-temperature-depth probe; CM = Nortek AquaDopp acoustic current meter; NIOZ-T = Royal Netherlands Institute for Sea Research thermistor chain attached to bottom lander. For the test data from the GoM limited information is available. Here σ_{max} is the maximum surface wind wave frequency measurable by the pressure sensors at mooring depth, calculated using linear wave theory. With N_1 the 90% percentile of the small-scale buoyancy frequency is meant here.

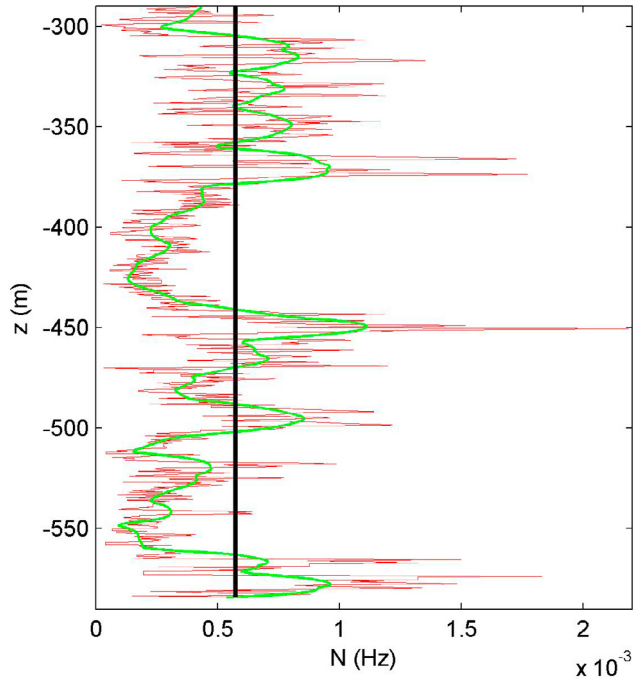

Figure 2. Sample buoyancy frequency profile from CTD observations near the Great Meteor Seamount (GMS) mooring. The buoyancy frequency is computed over different vertical scales: Δz = 1 m (red), Δz = 10 m (green), and Δz = 300 m (black).

(around $\langle H \rangle$) and $'$ variations around the time mean $\langle\ \rangle$. In p_{nh}, $\partial w/\partial t$ may replace Dw/Dt as they differ <10%, according to *Moum and Smyth* [2006]. Presumably their data were from relatively linear IW.

[8] From observations on a shelf [*Moum and Nash*, 2008], episodic, isolated events of nonlinear internal waves induce predominantly $|p_{ih}| \gg |p_{nh}|, |p_{eh}|$ with a negative pressure dip in p_{ih} of a solitary wave of depression and positive values for the weaker terms. However, following their analysis they state that in their monthly averaged spectra, hydrostatic surface wave pressure dominates over internal and nonhydrostatic pressures in the IWC. *Moum and Smyth* [2006] also indicate an independent estimate of internal wave pressure from horizontal near-bottom currents, assuming a constant phase speed c and propagation in x direction: $p' \sim \langle \rho \rangle$ cu. From this, one expects similar spectral characteristics for pressure and horizontal near-bottom currents. Indeed, horizontal current spectra from a neutral lower atmosphere show a similar shape of waves and turbulence as in Figure 1 [*Högström et al.*, 2002]. However, for a similar case *Hackett et al.* [2009] state that current observations include relatively more turbulence than pressure observations.

[9] In this paper we evaluate contributions of turbulence and internal waves in various ocean bottom pressure data with help of auxiliary high-resolution temperature and current data. It is noted that in (1) no specific turbulence terms are retained. These are unverifiable with the present data. All data are from sloping bottoms where one expects relatively large turbulence by (nonlinear) internal wave breaking; a much more dynamic environment than that of ubiquitous, but linear internal waves in the open ocean [*van Haren and Gostiaux*, 2009]. The primary aim is to investigate the possibility of observing IWC using bottom pressure, the secondary is the possibility of transition to turbulence.

2. Data

[10] Data from a variety of locations are used, ranging from a shallow and narrow sea strait (the Marsdiep, Netherlands) via the Baltic Sea and the open (Atlantic) ocean, near the tops of two guyots, to a deep Gulf of Mexico (GoM) site where during its deployment four large tropical storms/hurricanes passed with Dennis directly over it (the instrument was removed a month before Katrina passed over). Bottom topography is important for flow conditions at all sites. Environmental, flow and suspended matter, conditions vary considerably between the sites, which have water depths between 23 and 1932 m (Table 1). For all depth ranges, variations of 1 order in magnitude occur in current speed, in large vertical scale ($\Delta z \geq 100$ m; 'N') and small vertical scale ($\Delta z = 1$ m; 'N_1'; in spectra its 90% percentile will be indicated) buoyancy frequencies, as is confirmed using auxiliary data (Table 1). A typical example demonstrates large variation in stratification with depth (Figure 2), which is also observed as a function of time and space. The primary instrumentation however, is always the same: a bottom pressure recorder, with only slightly different settings depending on the experiment.

[11] Either a shallow water Sea-Bird Electronics (SBE) 26plus wave and tide recorder or a deep water SBE53 bottom pressure recorder is used. Both have a Digiquartz crystal, temperature-compensated pressure sensor with absolute accuracy of 10^{-4} of full-scale. The accurate (0.002°C), high-resolution (0.0001°C) temperature sensor and internal temperature compensation ensure a residual temperature sensitivity on pressure data which is less than 10^{-6} of full scale in the range 0–20°C (or <3.5 N m^{-2} °C^{-1} for the deepwater version).

[12] Crucial for pressure observations is the mounting at the bottom. A completely fixed structure is virtually impossible in harsh conditions like mainstream flows up to 1.5 m s^{-1} in the shallow Marsdiep. There, a nearly flat, lead-weighted frame is used with the sensor at 0.08 m above the bottom. In other deep-sea and ocean mountings a net 200 kg weighing bottom lander with acoustic Doppler current profiler (ADCP) is used. A 30–150 m long cable with high-resolution temperature sensors and current meters is attached to the lander. From tilt sensor information it is inferred that frame and lander occasionally vibrated slightly, thereby causing very high frequency pressure variations ("noise") up to 10 N m^{-2} under strong turbulence with occasional well-identified jumps reaching 20 N m^{-2} because of frontal passage.

[13] Frequency spectra were computed from entire record length time series observations. Averaging over half-overlapping data sections resulted in 3–15 degrees of freedom (dof) after applying a Kaiser (~cosine) taper window over each of the sections. The three main frequency bands IWC, IGW and SW were separated by band-pass filters applying sharp elliptic filters twice, thereby preserving phase. Filter bounds (at 10^{-4} falloff rate within a quarter of

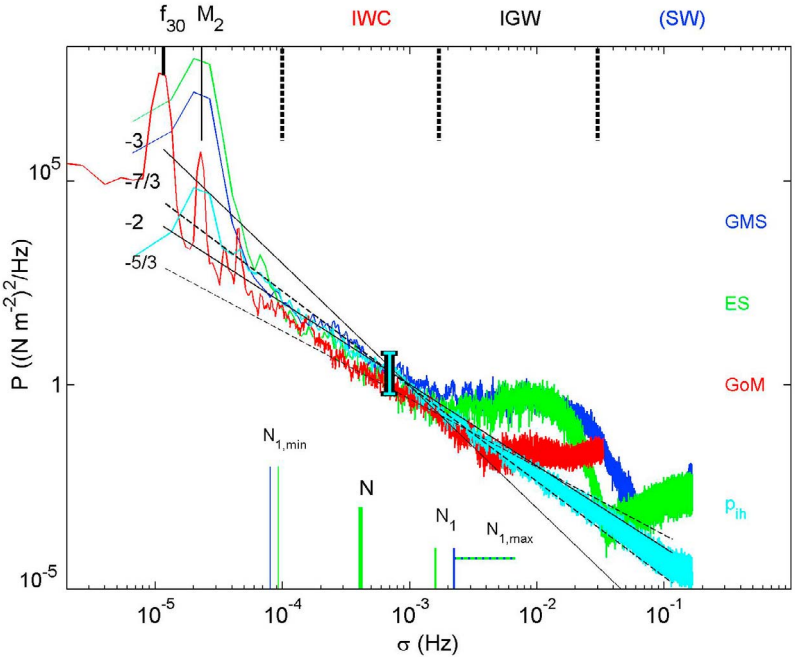

Figure 3. Bottom pressure spectra with $\Delta z = 1$ m minimum, $\Delta z = 300$ m mean, and $\Delta z = 1$ m 90% percentile and maximum buoyancy frequencies indicated by colored vertical bars in descending order. Three deep ocean sloping sites, GMS (blue), Equator Seamount (ES) (green) and Gulf of Mexico (GoM) (red), are compared with p_{ih} term in (1) estimated from temperature data above GMS (light blue). Four spectral slopes are given which, under a simple Taylor hypothesis transferring wave number to frequency space, may mimic internal waves (σ^{-2}, solid line [*Filloux*, 1980]), stratified turbulence (σ^{-3}, solid line), inertial (turbulent) convective subrange ($\sigma^{-5/3}$, dashed line; inferred from high wave number Kolmogorov spectrum of *Gotoh and Fukayama* [2001]), and inferred low wave number inertial turbulence pressure range ($\sigma^{-7/3}$, dashed line [*Gotoh and Fukayama*, 2001]). Slopes and blue GMS spectrum may be used for reference, as they are identical in Figures 3–5. The error bar indicates the mean 95% significance range. The vertically hanging black dashed lines indicate the filter bounds for bands IWC, IGW, and SW.

a decade) are given by dashed bars in Figures 3–5 discussed below.

3. Observations

3.1. Spectra

[14] In spite of 2 orders of magnitude differences in kinetic and potential (∼buoyancy) energy between the sites, a central frequency decade in bottom pressure spectra is near identical (to within ± half a decade or statistical uncertainty at the 95% significance level) in slope and amplitude: the decade between frequencies $10^{-4} < \sigma < 10^{-3}$ Hz (Figures 3–5). Within this band, the mean slope amounts -2.0 ± 0.2 and, to within the statistical uncertainty (the light blue bar in Figures 3–5 indicates its vertical extent at the 95% significance level), no distinction can be made between slopes varying from $-5/3$ to $-7/3$. It is remarkable that p spectra are so similar in this range, considering the different sites and their varying background conditions. This is postulated to represent IWC, following a comparison with an independent estimate of the dominant p_{ih}-term in (1).

[15] This internal hydrostatic pressure term is estimated from high-resolution temperature data at Great Meteor Seamount (GMS), albeit only in 0.5 m increments between 0.5 and 50 m above the bottom (mab). Transferring these data to density variations $\delta\rho = -0.101 \pm 0.002\delta$T using nearby conductivity-temperature-depth (CTD) data, and assuming the lower 100 m above the sloping bottom to contain most relevant density variations because of internal waves (as supported using current meter-temperature information up to 150 mab and given IW's maximum amplitude being approximately half that size), the light blue spectrum in Figure 3 is obtained. In the IWC it matches GMS bottom pressure spectra (blue), both in σ^{-2} slope and amplitude, and it continues to match them when the latter maintain the same spectral slope beyond $\sigma > 10^{-3}$ Hz, like for GoM data (red). This suggests bottom sensors have recorded pressure variations because of isopycnal displacements, at least in the IWC. Together with the spectral collapse, it also suggests saturation of IWC, thus representing an equilibrium transfer between sources, e.g., internal tides and near-inertial motions, and turbulent dissipation [*Phillips*, 1977]. *D'Asaro and Lien* [2000b] demonstrate for their model vertical wave number shear spectra that with increasing energy IWC shrinks at the expense of the turbulence bandwidth, while the IWC remains tight to its slope level.

[16] There are two more indications that IWC has thus been observed rather than surface waves or noise in this band.

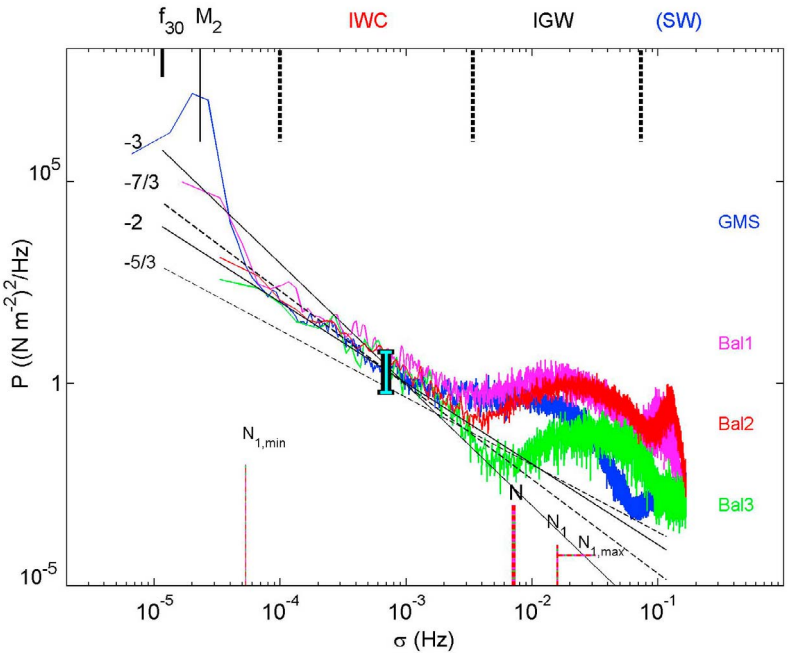

Figure 4. As Figure 3 but for Baltic Sea periods 1 (purple), 2 (red), and 3 (green).

These indications relate this band to particular independent variables, vertical current and stratification, which have typical form for IWC.

[17] First, spectra from vertical current observations using ADCP above GMS show a small peak just below N and roll-off just to about the upper limit of the above IWC range obtained from pressure observations, indicative of and coinciding with N_1 (Figure 6, red spectrum). This is because small-scale, thin layer internal wave motions dominate vertical currents; near N-N_1 the aspect ratio of motions is about equal to one and a small peak in w spectra is commonly found [e.g., *Cairns*, 1975], which has a shape similar to the stratification distribution [*van Haren and Gostiaux*, 2009]. In the open ocean, the shape slopes like σ^{+1} from IWC toward N [*van Haren and Gostiaux*, 2009], whereas in other, probably more turbulent, areas it slopes more like σ^0 [*D'Asaro and Lien*, 2000a]. Here, the effect of stratification is visible as a second insignificant submaximum is found at

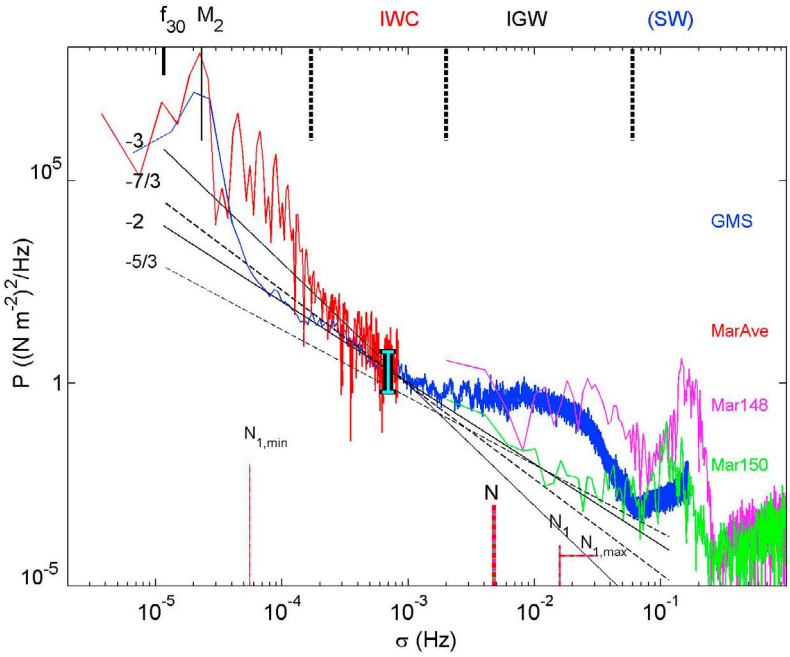

Figure 5. As Figure 3 but for Marsdiep ('Mar') 500 s burst examples on days 148.2 (purple) and 150.16 (green), and 600 s averages (red).

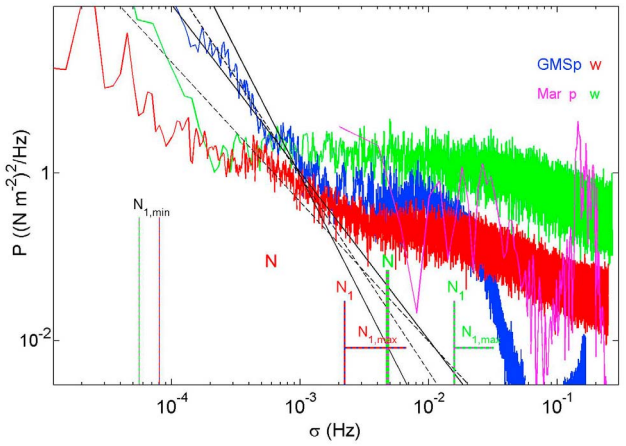

Figure 6. Blowup of the same blue (GMS) and purple (Marsdiep) spectra as in Figure 5, compared with vertical current spectra (arbitrary scale) from GMS (red) and Marsdiep (green).

max(N_1) ($\sigma \sim 7 \times 10^{-3}$ Hz) before another roll-off, steeper for pressure (blue), commences at σ = 2–3 $\times$ 10^{-2} Hz, about the upper limit of IGW. Near-bottom Marsdiep w spectra only roll-off at the latter, commensurate the (periodically) more than one decade larger N_1.

[18] Second, CTD data confirm w spectral roll-off by the ranges of both large-scale N and small-scale N_1. These differ, but large-scale N more or less indicates the high-frequency limit of IWC, except for short periods over which spectra may extend to N_1, like for the Marsdiep example, on day 150. The low-frequency IWC limit coincides with the min(N_1) rather than canonical f, as above sloping bottoms tidal (higher) harmonic motions flowing up and down disturb IWC. Remains to explain the p,w roll-off for σ > N, (N_1) that is beyond IWC and part of IGW. This is discussed next.

[19] Bottom pressure spectra do differ in amplitude and (slightly) in frequency range of the broad bulge that characterizes IGW (Figures 1 and 3–5). As mentioned above for GMS and Marsdiep, IGW partially coincides with maximum N_1 range and with the high-frequency extent of measurable vertical currents before rolling off to noise (Figure 6). The latter currents may represent very high frequency internal waves supported by extremely large thin layer stratification (which also are observed in the Baltic) but also large-scale turbulent overturns. These overturns are generated by the tide flowing up and down sloping topography, whether sand dunes like in the Marsdiep or larger scale like above guyots, thereby generating boils in the water, apparently typically lasting 30–60 s [*Nimmo Smith et al.*, 1999; *van Haren*, 2010]. The same time scale is found for ubiquitous turbulent motions in the interior over GMS, culminating in Kelvin-Helmholtz overturns of 5–10 m height [*van Haren and Gostiaux*, 2010]. The shortest-scale internal waves observed in the Baltic are mostly (local) mode 2, like K-H billows, with 30–60 s periods. As a result, the IGW bulge seems dominated in the present observations by nonlinear small-scale internal wave motions in their transition to largest turbulent scales: direct evidence of buoyancy subrange of stratified turbulence [*Riley and Lindborg*, 2008].

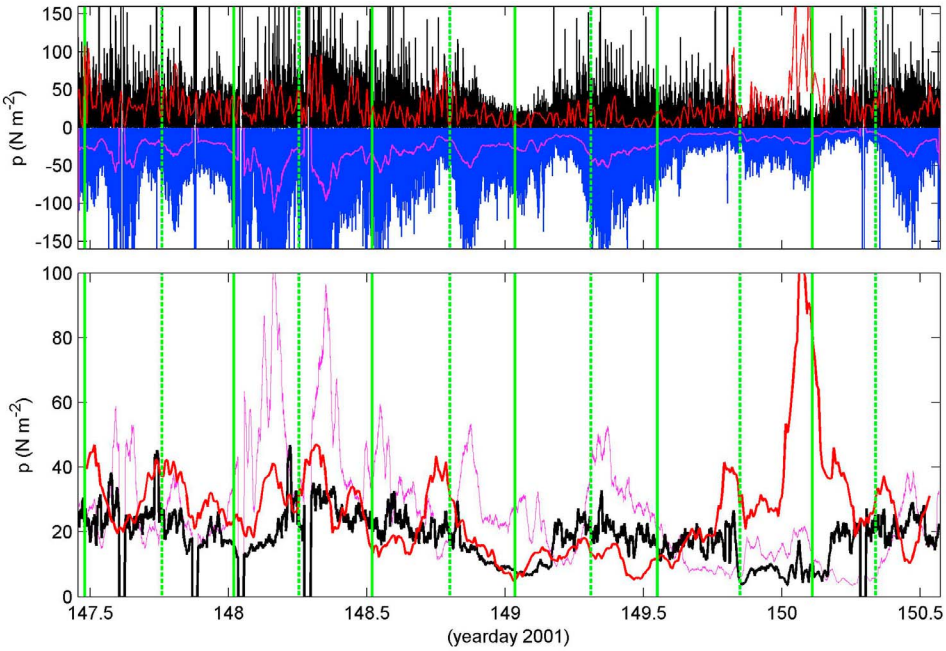

Figure 7. (top) Time series of band-pass filtered Marsdiep bottom pressure for IWC (red), IGW (black), and SW plus instrumental noise (blue). In green tidal rhythm of low (dashed) and high water (solid). In purple the (negative value of) 1.7 h smoothed square root SW variance is given. (bottom) The 1.7 h smoothed square root variance of IWC (red), IGW (black) and SW (purple; same as negative in Figure 7, top).

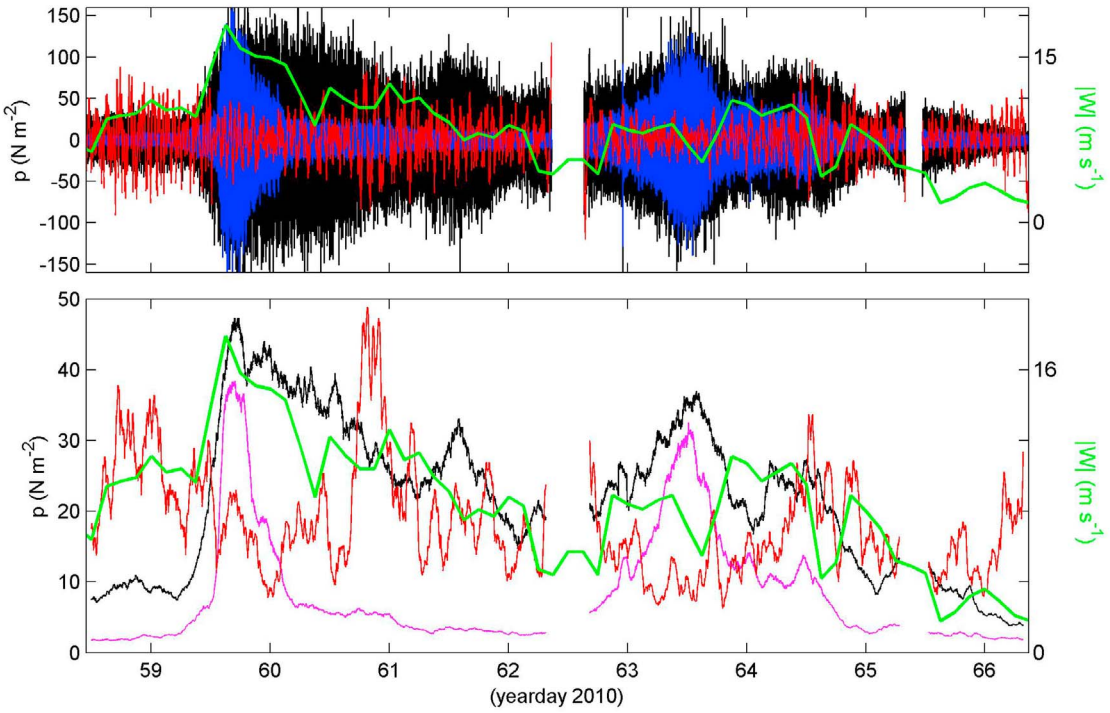

Figure 8. As in Figure 7 but for Baltic, in green wind speed (scale to right).

3.2. Band-Pass Filtered Time Series

[20] The above suggested transition to turbulence may vary between environments, with different dominant sources as may be inferred by comparing band-pass filtered bottom pressure time series of IWC (red), IGW (black) and SW + high-frequency noise (blue or purple) with additional source, e.g., tidal and wind, information (green) (Figures 7–11). What strikes most in all environments is that IWC and IGW show enhanced values generally at different times in the records, regardless the forcing. This not only occurs on the large, mesoscale of a week and longer, but also on daily time scales. The present data records are too short for rigorous

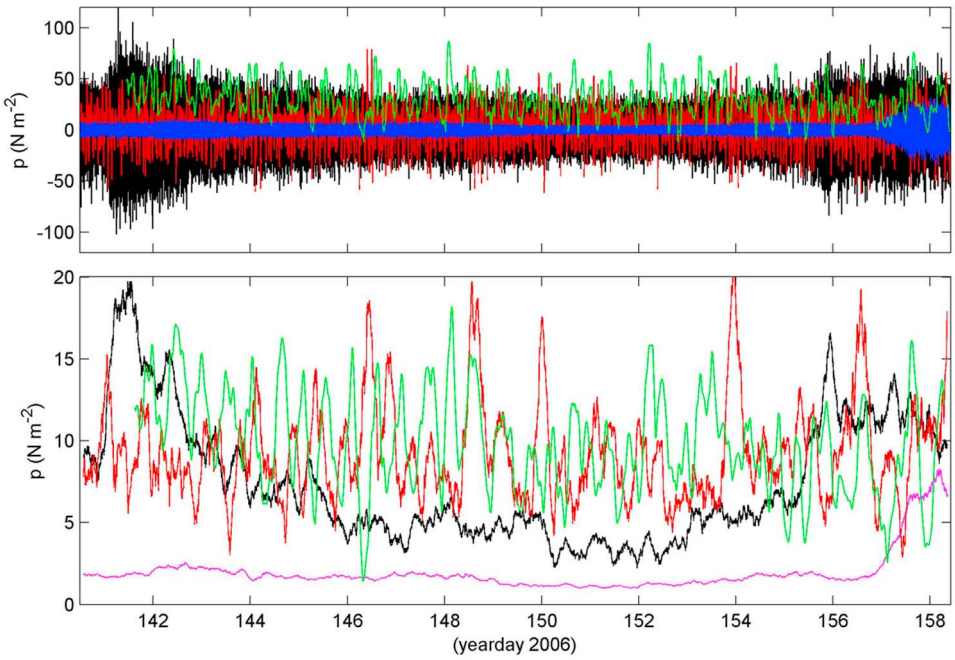

Figure 9. (top) As in Figure 7 but for GMS (different pressure range), in green log(ε) (arbitrary scale). (bottom) IWC (red) and IGW (black) are offset vertically for better comparison.

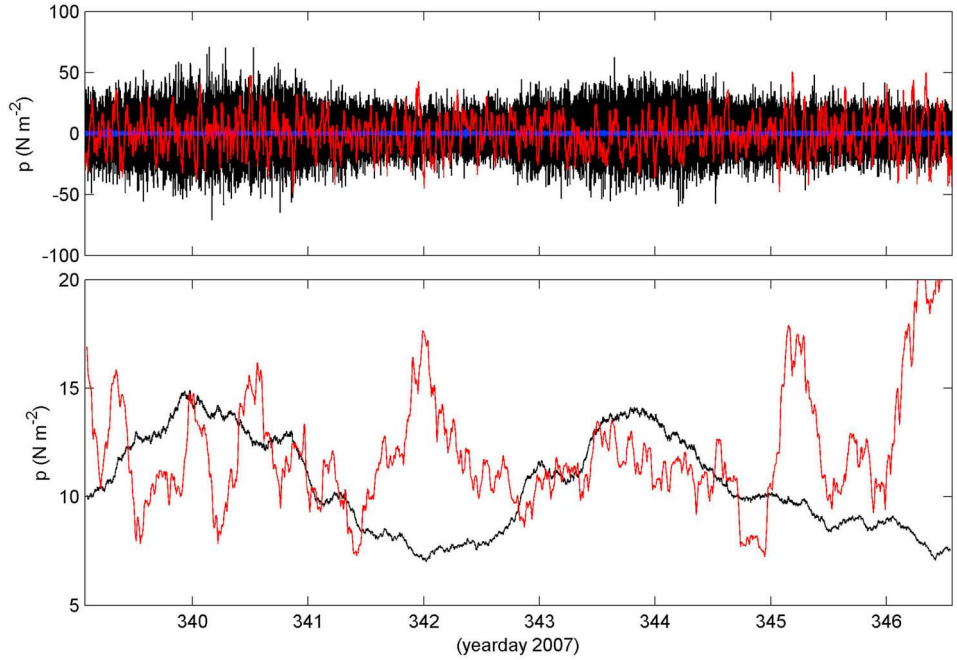

Figure 10. (top) As in Figure 7 but for ES (different pressure range). (bottom) Smoothing of 5 h is applied and SW is omitted (noise only).

statistical analysis at these time scales. It is debatable whether statistically meaningful relationships can be found even in longer data sets, as neither IWC nor IGW are a source or a permanent sink, but rather intermediates.

[21] In the Marsdiep the semidiurnal tide is dominant, and IWC varies accordingly, showing submaxima at most low waters (Figure 7). IGW has a diurnal variability, which is partially due to wind variations as SW shows similar variability; partially it is due to bubble clouds induced by daytime only (day 167 and day 183) ferry passages [*van Haren*, 2009].

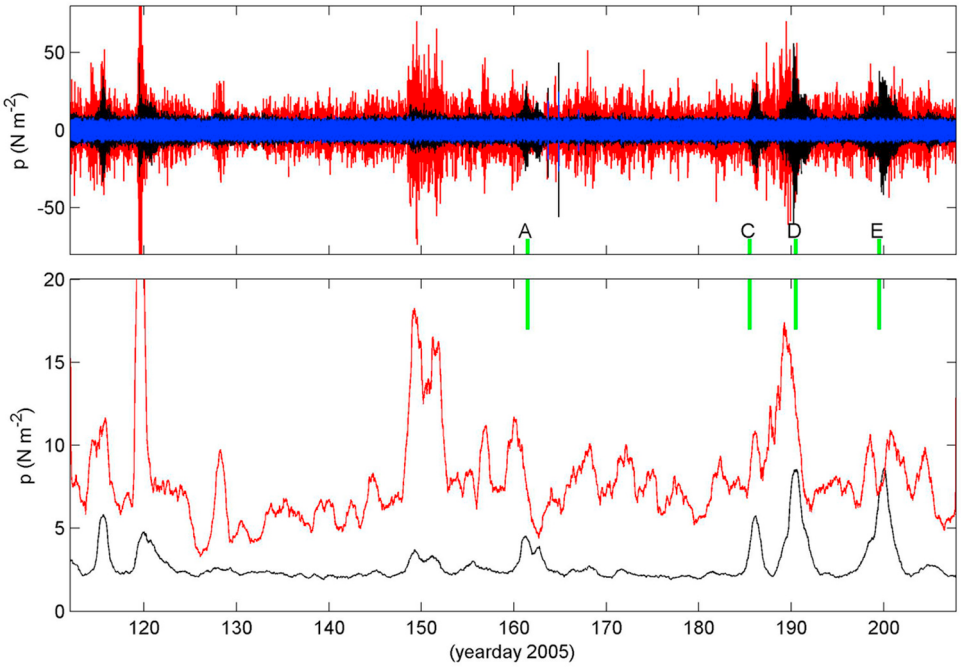

Figure 11. (top) As in Figure 7 but for GoM (different pressure range), in green Gulf passages of tropical storms/hurricanes. Tropical storm Arlene and Hurricane Emily passed at considerable distance from the mooring site, whereas hurricanes Cindy and especially Dennis passed directly over mooring. All storms approached from the south. (bottom) Smoothing of 1 d is applied and SW is omitted (noise only).

[22] In the Baltic (Figure 8) where tides are relatively weak and main energy input is through wind via inertial motions, IGW follows wind bursts manifest in SW peaks, but not always (e.g., day 61 following large IWC). IWC has no relation with wind, but alternates with IGW at 1.8–2 d and 3–4 d periodicities and a phase lag of about 1 d.

[23] Above GMS (Figure 9), tidal variations are found in IWC, which are regularly inversely related to predominantly tidally varying turbulent kinetic energy dissipation rate ε (green) estimated from overturns in high-resolution Royal Netherlands Institute for Sea Research thermistor data. Some coherence is found in the M_2 and M_4 (visible as rapid double peaks in the green curve in Figure 9, top) tidal bands, with 180° phase difference, but at ~75% confidence levels only. Conversely, IGW shows a fortnightly (spring-neap) variation, but not tidal variations. No relationship is observed between IWC and SW (blue), which is not surprising given the 550 m water depth at which most SW are attenuated to below pressure sensor noise level (Table 1). On an intermediate 3–4 d scale IGW and IWC alternate.

[24] This 3–4 d time scale is also apparent at greater depths, predominantly in IGW for the equatorial guyot, modulating a semidiurnal tidal periodicity for IWC (Figure 10), and in IWC for GoM (modulated with diurnal tidal/inertial variations) (Figure 11). IWC- Equator Seamount (ES) clearly alternates (180° phase difference) with IGW-ES at the 3–4 d time scale. For the long time series of GoM some coherence is found in this band between IWC and IGW, but at 85% confidence level only (not shown). It is noted that IWC-GoM is not specifically related to (distinct or local) passages of hurricanes, but IGW-GoM more so. However, unexplained are variations from zero phase difference between IGW peak and passages (Dennis pass over, Emily remote pass, for example) and delays by days (Cindy pass over). Note the near-complete extinction of large IWC activity and increasing IGW when Dennis passes over. Also, both simultaneously enhanced and alternating-enhanced IGW and IWC are observed earlier in the year, prior to the tropical storm season.

4. Discussion

[25] The observed collapse of sloping bottom pressure spectra in the frequency range $10^{-4} < \sigma < 10^{-3}$ Hz suggests a saturated core of IWC. Tidal modulation of IWC bottom pressure time series partially supports this, as tides are a prominent source of internal waves especially above sloping topography. Another source are atmospheric disturbances and inertial waves. Further support is obtained from spectral match with internal hydrostatic pressure estimated using independent temperature data. All observations have been made in areas where nonlinear internal wave propagation becomes near-critical, so that waves' particle and phase speeds match, as above sloping bottoms and in shallow seas. As a result, the present observations resemble the Lagrangean observations by *D'Asaro and Lien* [2000a, 2000b] and the isopycnal slope spectra by *Klymak and Moum* [2007], who found no variation in the IW subrange despite 4 orders of magnitude variations in turbulence dissipation. The wave-turbulence model of shear suggested by *D'Asaro and Lien* [2000a, 2000b] well represents (in form) Figure 1 here, implying that internal waves and turbulence are coupled. The sharp but gapless (or small gap) transition between IWC and IGW allows many small-scale internal waves to exist besides turbulence in IGW, especially at the shallow sites as is supported by present w spectra. As these motions are not manifest of long surface waves, a modified interpretation of IGW bottom pressure spectra is suggested for sloping topography as italicized in Figure 1 and to call it 'internal wave-turbulence' (IWT).

[26] Long surface gravity waves occupy the same frequency range as IWT and they partially have the same sources in atmospheric disturbances, which make them hard to distinguish from each other. A few suggestions are given for their distinction in the IGW/IWT band, outside (the influence of) sloping topography areas. First, O(10–100) m above the bottom internal wave turbulence decreases rapidly, so that long surface waves may dominate pressure observations. Second, near its sources and in enclosed seas like the Baltic the dispersive character of long surface waves may be in a different stage of development compared to far from its source and in the open ocean. As a result, the spectral shape will be different, in contrast with the equilibrium surface wave spectrum. Third, if long surface waves would dominate IGW/IWT, they unlikely couple (in phase or alternating) with IWC, because the latter have different sources in, e.g., tides and which are highly modified by variations in stratification that do not affect long surface waves.

[27] An ideal measurement setup to robustly investigate potential coupling between IWC and IGW bands would involve a short-scale spatially three-dimensional instrumental array. Typical scales to be resolved are O(1 m) vertically and O(10 m) horizontally, over ranges O(100 m). Typical instruments to be used are temperature sensors, 3-D turbulence-current meters and, at the bottom, pressure sensors. Deployment of this array requires a formidable logistics operation, besides a considerable amount of instrumentation. Besides the above coupling, the setup may be used for studying internal wave propagation under a variety of (incoming) angles. The array should also be deployed in the more quiescent interior, for comparison.

[28] **Acknowledgments.** I enjoyed the assistance of the crews of the R/V *Pelagia*, R/V *Navicula*, and R/V *Alkor* (principal investigator Lars Umlauf). Theo Hillebrand and Martin Laan helped preparing the instrumentation. I thank Darius Miller of SBE for investigation of their Gulf of Mexico data.

References

Bromirski, P. D., and P. Gerstoft (2009), Dominant source regions of the Earth's "hum" are coastal, *Geophys. Res. Lett.*, *36*, L13303, doi:10.1029/2009GL038903.

Cairns, J. (1975), Internal wave measurements from a midwater float, *J. Geophys. Res.*, *80*, 299–306, doi:10.1029/JC080i003p00299.

D'Asaro, E. A., and R.-C. Lien (2000a), Lagrangian measurements of waves and turbulence in stratified flows, *J. Phys. Oceanogr.*, *30*, 641–655, doi:10.1175/1520-0485(2000)030<0641:LMOWAT>2.0.CO;2.

D'Asaro, E. A., and R.-C. Lien (2000b), The wave-turbulence transition for stratified flows, *J. Phys. Oceanogr.*, *30*, 1669–1678, doi:10.1175/1520-0485(2000)030<1669:TWTTFS>2.0.CO;2.

Filloux, J. H. (1980), Pressure fluctuations on the open ocean floor over a broad frequency range: New program and early results, *J. Phys. Oceanogr.*, *10*, 1959–1971, doi:10.1175/1520-0485(1980)010<1959:PFOTOO>2.0.CO;2.

Gotoh, T., and D. Fukayama (2001), Pressure spectrum in homogeneous turbulence, *Phys. Rev. Lett.*, *86*, 3775–3778, doi:10.1103/PhysRevLett.86.3775.

Hackett, E. E., L. Luznik, J. Katz, and T. R. Osborn (2009), Effect of finite resolution on the turbulent energy spectrum measured in the coastal ocean bottom boundary layer, *J. Atmos. Oceanic Technol.*, *26*, 2610–2625, doi:10.1175/2009JTECHO647.1.

Herbers, T. H. C., S. Elgar, R. T. Guza, and W. C. O'Reilly (1995), Infragravity-frequency (0.005–0.05 Hz) motions on the shelf. Part II: Free waves, *J. Phys. Oceanogr.*, *25*, 1063–1079, doi:10.1175/1520-0485(1995)025<1063:IFHMOT>2.0.CO;2.

Högström, U., J. C. R. Hunt, and A.-S. Smedman (2002), Theory and measurements for turbulence spectra and variances in the atmospheric neutral surface layer, *Boundary Layer Meteorol.*, *103*, 101–124, doi:10.1023/A:1014579828712.

Klymak, J. M., and J. M. Moum (2007), Oceanic isopycnal slope spectra. Part I: Internal waves, *J. Phys. Oceanogr.*, *37*, 1215–1231, doi:10.1175/JPO3073.1.

Longuet-Higgins, M. S., and R. W. Stewart (1964), Radiation stress in water waves: A physical discussion, with applications, *Deep Sea Res.*, *11*, 529–562.

Moum, J. N., and J. D. Nash (2008), Seafloor pressure measurements of nonlinear internal waves, *J. Phys. Oceanogr.*, *38*, 481–491, doi:10.1175/2007JPO3736.1.

Moum, J. N., and W. D. Smyth (2006), The pressure disturbance of a nonlinear internal wave train, *J. Fluid Mech.*, *558*, 153–177, doi:10.1017/S0022112006000036.

Nimmo Smith, W. A. M., S. A. Thorpe, and A. Graham (1999), Surface effects of bottom-generated turbulence in a shallow tidal sea, *Nature*, *400*, 251–254, doi:10.1038/22295.

Okihiro, M., and R. T. Guza (1995), Infragravity energy modulation by tides, *J. Geophys. Res.*, *100*, 16,143–16,148, doi:10.1029/95JC01545.

Phillips, O. M. (1977), *Dynamics of the Upper Ocean*, 2nd ed., 336 pp., Cambridge Univ. Press, Cambridge, U. K.

Riley, J. J., and E. Lindborg (2008), Stratified turbulence: A possible interpretation of some geophysical turbulence measurements, *J. Atmos. Sci.*, *65*, 2416–2424, doi:10.1175/2007JAS2455.1.

Uchiyama, Y., and J. C. McWilliams (2008), Infragravity waves in the deep ocean: Generation, propagation, and seismic hum excitation, *J. Geophys. Res.*, *113*, C07029, doi:10.1029/2007JC004562.

van Haren, H. (2009), Ship-induced effects on bottom-mounted acoustic current meters in shallow seas, *Cont. Shelf Res.*, *29*, 1809–1814, doi:10.1016/j.csr.2009.06.002.

van Haren, H. (2010), Very near-bottom tidal straining in a sea strait, *Geophys. Res. Lett.*, *37*, L16603, doi:10.1029/2010GL044186.

van Haren, H., and L. Gostiaux (2009), High-resolution open-ocean temperature spectra, *J. Geophys. Res.*, *114*, C05005, doi:10.1029/2008JC004967.

van Haren, H., and L. Gostiaux (2010), A deep-ocean Kelvin-Helmholtz billow train, *Geophys. Res. Lett.*, *37*, L03605, doi:10.1029/2009GL041890.

Webb, S. C. (1998), Broadband seismology and noise under the ocean, *Rev. Geophys.*, *36*, 105–142, doi:10.1029/97RG02287.

H. van Haren, Physical Oceanography, Royal Netherlands Institute for Sea Research, PO Box 59, Den Burg, Texel 1790 AB, Netherlands. (hans.van.haren@nioz.nl)